Electronic Supplementary Material (ESI) for Journal of Materials Chemistry A.

Electronic Supplementary Information

Tailoring electrochemical CO_2 reduction via substrate-induced gas diffusion

Younghyun Chae[a,b‡], Kyeongsu Kim[a‡], Hyewon Yun[c], Dongjin Kim[a,d], Wonsang Jung[a,b], Yun Jeong Hwang[c,e], Ung Lee[a,b,f], Dong Ki Lee[a,b,f,g], Byoung Koun Min[a,f], Woong Choi[a,*], and Da Hye Won[a,b,*]

[a]Clean Energy Research Center, Korea Institute of Science and Technology, Seoul 02792, Republic of Korea

[b]Division of Energy and Environmental Technology, KIST School, Korea University of Science and Technology (UST), Seoul 02792, Republic of Korea

[c]Department of Chemistry, Seoul National University, Seoul 08826, Republic of Korea

[d]Department of Materials Science and Engineering, Korea University, Seoul 02841, Republic of Korea

[e]Center for Nanoparticle Research, Institute for Basic Science (IBS), Seoul 08826, Republic of Korea

[f]Graduate School of Energy and Environment (Green School), Korea University, Seoul 02841, Republic of Korea

[g]Department of Chemical and Biomolecular Engineering, Yonsei-KIST Convergence Research Institute, Yonsei University, Seoul 03722, Republic of Korea

‡These authors contributed equally to this work

AUTHOR INFORMATION

Corresponding author(s)

Woong Choi – E-mail: nayacu@lbl.gov

Da Hye Won – E-mail: dahye0803@kist.re.kr

Table of contents

Supplementary Notes

Supplementary Figures

Fig. S1-S12

Supplementary Tables

Table S1-S3

Supplementary References

Supplementary Notes

Computational details

The 2-D H-type model is drawn using the COMSOL Multiphysics reflecting the actual devices. The model is composed of the electrolyte region in liquid phase, the CO gas region in gas phase, and the permeable media indicating the carbon paper (CP) or glassy carbon (GC) substrates. The 2-D geometry of the simulation model can be seen in Fig. 3b. The CO gas is fed into the cell in the corner of the gas phase region of the H-type cell in the flow rate of 20 ml m^{-1}.

The fluidic motion in the gas phase region of the cell is expected to be governed by convection flowing from the entrance to the exit located on the top of the cell. Also, diffusion can affect the transport of CO in the gas region. Thus, the convection-diffusion model to consider the combined effect in CO transport.

$$\nabla \cdot \boldsymbol{J}_{CO} + \boldsymbol{u}_{CO} \cdot \nabla c_{CO} = 0 \quad (1)$$

where $\boldsymbol{J}_{CO} = -D_{CO}\nabla c_{CO}$. Note that this study considers a simple stationary calculation to check if CO can be delivered to the substrate-catalyst interface through the substrates, thus the time-dependent and reaction terms are omitted in Eq. (1) and the rest of the equations in this paper. $\boldsymbol{J}_{CO}$, $\boldsymbol{u}_{CO}$, and c_{CO} are indicating the CO mass flux, CO gas velocity, and CO concentration, respectively. The diffusion coefficient of CO is set as 2.08×10^{-5} under the assumption that the conditions inside the cell were maintained at atmospheric pressure and 20°C. The initial value for the CO velocity was set as 0 and the CO concentration was assumed to be 40.9 mol m^{-3} to consider the case that the cell is initially filled with CO gas under atmospheric pressure. The initial concentrations of CO in both CP and GC are assumed to be 0. The velocity, $\boldsymbol{u}_{CO}$, in the gas phase region is governed by the Navier-Stokes and the continuity equation.

$$\rho(\boldsymbol{u} \cdot \nabla)\boldsymbol{u} = \nabla \cdot \left[-p\boldsymbol{I} + \mu(\nabla\boldsymbol{u} + (\nabla\boldsymbol{u})^{\mathrm{T}}) - \frac{2}{3}\mu(\nabla \cdot \boldsymbol{u})\boldsymbol{I}\right] + \rho\boldsymbol{g} = 0 \quad (2)$$

$$\nabla(\rho\boldsymbol{u}) = 0 \quad (3)$$

where ρ and μ indicate the mass density and the dynamic viscosity of CO gas of which values are 1.12 kg m^{-3} and $1.74\ \times 10^{-5}$ Ns m^{-2} under the conditions of atmospheric pressure and 20°C.

When the CO gas flows through the CP substrate, the mass transport follows the Darcy's law, which describes the flow in a porous medium using the permeability of the medium, k and the pressure drop, ∇p.

$$\boldsymbol{u} = -\frac{k}{\mu}\nabla p \qquad (4)$$

The constructed model sets k as 8.4×10^{-12} m^2 considering the in-plane permeability of Sigracet 39BB GDL, which was utilized in actual CO reduction reaction (CORR) experiment.[1] For the flows in porous media, the mass and momentum conservation equation should be modified considering the porosity, ϵ, and the permeability, k.

$$\frac{1}{\epsilon}\rho(\boldsymbol{u}\cdot\nabla)\boldsymbol{u}\frac{1}{\epsilon} = \nabla\cdot\left[-p\boldsymbol{I} + \mu\frac{1}{\epsilon}(\nabla\boldsymbol{u} + (\nabla\boldsymbol{u})^{\mathrm{T}}) - \frac{2}{3}\mu\frac{1}{\epsilon}(\nabla\cdot\boldsymbol{u})\boldsymbol{I}\right] - \left(\frac{\mu}{k} + \frac{Q_m}{\epsilon^2}\right)\boldsymbol{u} + \rho\boldsymbol{g} = 0 \quad (5)$$

$$\nabla(\rho\boldsymbol{u}) = Q_m \quad (6)$$

where Q_m indicates the mass source term in the unit of kg m^{-3} s^{-1}. The porosity of CP is set as 0.83 according to a published study on the porosities of carbon papers.[2]

In the case of GC substrate, the flow equations for the porous media can no longer be applied due to the fact that there are no open pores in GC. However, CO gas transport through the GC substrate can still be modelled by the solution-diffusion equation.[3] The solution-diffusion theory states that a small amount of fluid is dissolved in the nonporous media first, and then diffuses through the media. In other words, the gas component in the gas phase region goes through the transport process in the order of adsorption at the entrance of GC, diffusion inside the GC, and desorption at the outlet to reach the substrate-catalyst interface. Studies on the mass transport through the glassy membranes and polymers often indicate the transport property of a specific component through nonporous media using the combined term of the solubility of gas components and the diffusion coefficient in the nonporous media. Using the solution-diffusion model, the CO permeability through the GC can be written as,

$$P_{CO,GC} = H_{CO,GC} \times D_{CO,GC} \quad (7)$$

where $P_{CO,GC}$, $H_{CO,GC}$, and $D_{CO,GC}$ indicate the CO permeability through GC, the CO solubility in GC, the CO diffusion coefficient in GC, respectively. The diffusion coefficient, $D_{CO,GC}$, is set as 1×10^{-12} m^2 s^{-1} according to the technical report on GC permeability,[4] but unfortunately, the values for $P_{CO,GC}$ and $H_{CO,GC}$ can hardly be found in published literature. In addition, estimating $H_{CO,GC}$ value directly from experiment, thus the studies aim at estimating the permeability in the unit of 'barrer' or '$\frac{\mathrm{m_{STP}^3 \cdot m}}{\mathrm{m^2 \cdot s \cdot kPa}}$'. Although finding CO permeability through GC is not available, we assumed that $P_{CO,GC}$ is $0.4 \times 10^{-14} \frac{\mathrm{m_{STP}^3 \cdot m}}{\mathrm{m^2 \cdot s \cdot kPa}}$ referring to the published study on a glassy membrane.[5] In the CFD simulation model, the solubility should only be applied to the surface of the GC entrance to make a difference between the CO concentrations in the gas phase region and the GC substrate. Accordingly, in place of $H_{CO,GC}$, the partition coefficient defined by the ratio of the CO concentration in GC over that in the gas phase region is calculated using Eq. (7) and applied to the GC entrance.

The pressure at the gas outlet is fixed at the atmospheric pressure. For all the walls including the inner walls, which indicate the sealed side of the substrate, no slip and no flux conditions are applied. A total of 12,315 mesh elements generated by COMSOL Multiphysics were used for calculation.

The CFD model constructed in this study utilized the geometry projected onto 2-D space, thus calculating the mass flow rate at the boundaries requires the flow rate terms that can be defined in 2-D space. First, the model should satisfy the following mass balance defined using the line integrals of the total fluxes.

$$\int_{\partial\Omega_{\mathrm{in}}} (\nabla \cdot \boldsymbol{J}_{CO} + \boldsymbol{u}_{CO} \cdot \nabla c_{CO}) \cdot \boldsymbol{n}\, \mathrm{d}S + \int_{\partial\Omega_{\mathrm{out}}} (\nabla \cdot \boldsymbol{J}_{CO} + \boldsymbol{u}_{CO} \cdot \nabla c_{CO}) \cdot \boldsymbol{n}\, \mathrm{d}S$$

$$+ \int_{\partial\Omega_{\mathrm{s}}} (\nabla \cdot \boldsymbol{J}_{CO} + \boldsymbol{u}_{CO} \cdot \nabla c_{CO}) \cdot \boldsymbol{n}\, \mathrm{d}S = 0 \quad (8)$$

where $\boldsymbol{n}$ is the normal vector. The subscripts in, out, and s in Eq. (8) indicate the model boundaries for the CO gas inlet and outlet of the cell, and the substrate-catalyst interface. Note that the CFD model considers that the CO reaching the substrate-catalyst interface leaves the system boundary, thus the interface should be treated as an outlet boundary. The CO mass flow rate at the substrate-catalyst boundary, $\dot{m}_\mathrm{s}$, can be calculated using the terms in Eq. (8) and the CO inlet flow rate ($\dot{m}_\mathrm{in}$=3.75 kg s^{-1}).

$$\dot{m}_s = \dot{m}_\mathrm{in} \frac{\int_{\partial\Omega_\mathrm{s}} (\nabla \cdot \boldsymbol{J}_{CO} + \boldsymbol{u}_{CO} \cdot \nabla c_{CO}) \cdot \boldsymbol{n}\, \mathrm{d}S}{\int_{\partial\Omega_\mathrm{in}} (\nabla \cdot \boldsymbol{J}_{CO} + \boldsymbol{u}_{CO} \cdot \nabla c_{CO}) \cdot \boldsymbol{n}\, \mathrm{d}S} \quad (9)$$

The CO gas flowing out at the CP-catalyst interface was estimated as 4.32$\times 10^{-9}$ kg s^{-1}. On the contrary, the estimated CO gas leaving at the GC-catalyst interface was 2.5$\times 10^{-16}$ kg s^{-1}. Assuming that all CO delivered to catalyst is converted to ethylene by CORR, the maximum CO partially current density can be calculated using the following equation.

$$j_{co,max} = \frac{z\dot{m}_s F}{A w_{CO}} \quad (10)$$

where z, F, A, and w_{CO} indicate the number of required electron for CORR (z = 6), Faraday constant, active catalyst area (0.3 cm^2), and CO molecular weight, respectively. According to Eq. (10), $j_{co,max}$ for CP and GC substrates would be limited up to 2.95$\times 10^{2}$ and 1.71$\times 10^{-5}$ mA cm^{-2}. This results imply that CP can serve as a pathway to deliver an enough amount of CO to the catalyst for CORR, however, it is highly unlikely to experimentally observe ethylene produced by reduction reaction of CO delivered through GC substrate.

Electrochemical surface area (ECSA)

ECSAs were analyzed by lead underpotential deposition on Cu on electrodes in perchloric acid.[6] Electrodes were activated and stabilized in 0.1 M $HClO_4$ solution at -0.4 $V_{Ag/AgCl}$ for 20 min. Then cyclovoltammetry between 1.0 to -0.5 $V_{Ag/AgCl}$ was conducted at 5 mV s^{-1} in 0.1 M $HClO_4$ + 1 mM $Pb(ClO_4)_2$ solution. The lead underpotential peaks appeared at -0.2 to -0.1 V_{RHE} and the peaks were integrated and divided by monolayer Pb atom coverage over Cu with a conversion factor of 310 μC cm^{-2}.

Ferricyanide reduction

Mass-transfer limitations were measured by ferricyanide ($K_3Fe(CN)_6$) reduction on each electrode. Ferricyanide reduction is known as the ideal reaction to show mass-transfer limitation since the reaction is so fast and easy that the observed rate is determined only by mass-transfer regardless of the applied potential.[7] LSVs of each electrode with and without 10 mM ferricyanide in 0.1M $KHCO_3$ were scanned at 1.0 $V_{Ag/AgCl}$ to -1.0 $V_{Ag/AgCl}$ with 5 mV s^{-1} scan rate. Mass-transfer was decided at 0.2 to 0.4 $V_{Ag/AgCl}$ where CO_2RR did not occur and the current rarely flowed, while ferricyanide reduction proceed.

Supplementary Figures

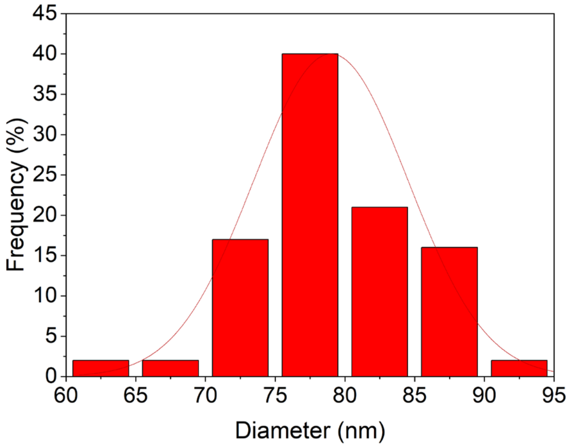

Fig. S1 Particle size histogram of the synthesized Cu_2O nanocubes (79 ± 5.5 nm).

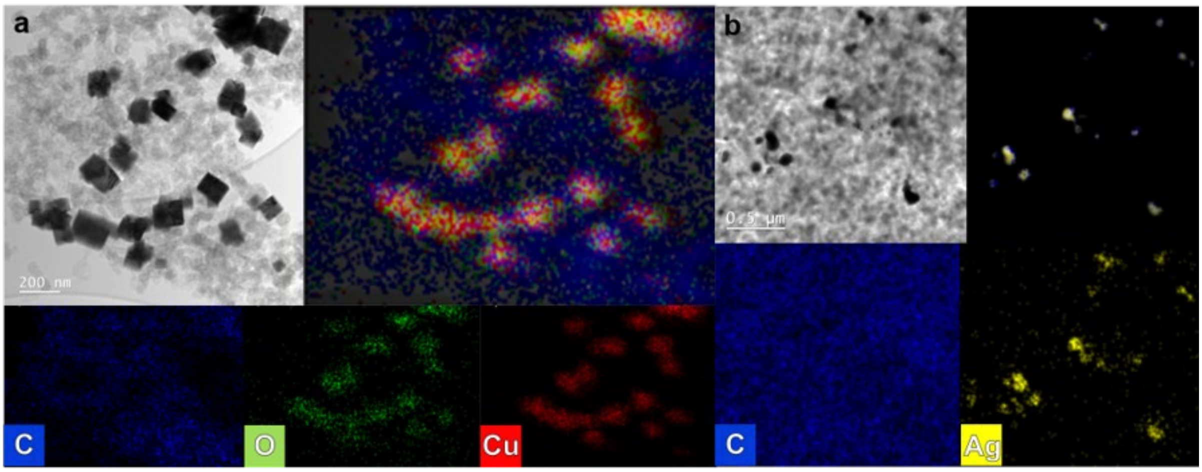

Fig. S2 TEM image and EDX mapping of (a) carbon anchored Cu_2O nanocubes and (b) carbon anchored Ag nanoparticles. Colored dots indicate each element, carbon (blue), oxygen (green), copper (red), and silver (yellow).

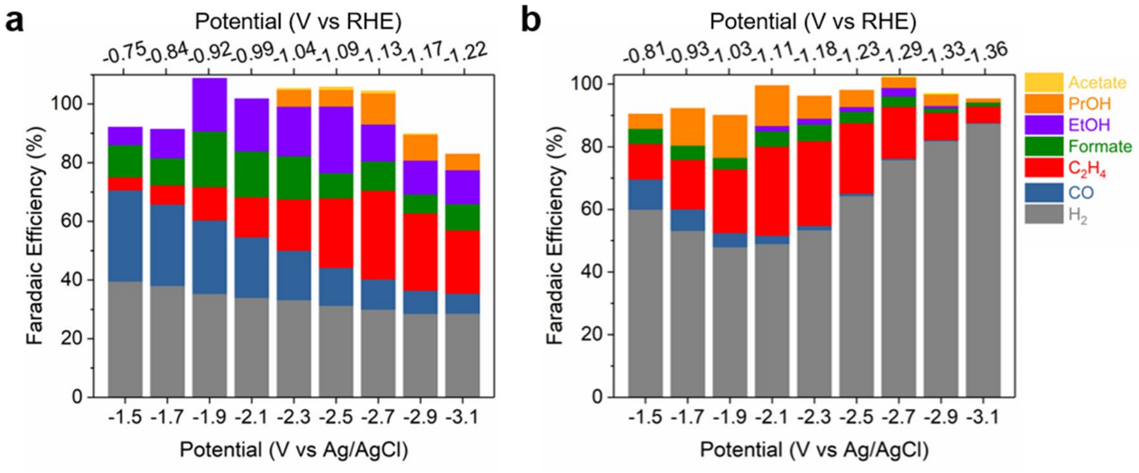

Fig. S3 CO_2RR performance of Cu catalyst depending on the substrates indicating every independent product. Faradaic efficiencies of H_2 (gray), CO (blue), C_2H_4 (red), formate (green), ethanol (violet), propanol (orange), and acetate (yellow) of Cu catalysts deposited on (a) CP and (b) GC at various potentials from -1.5 to -3.1 V vs. Ag/AgCl in CO_2-bubbled 0.1 M $KHCO_3$. Each potential was converted to reversible hydrogen electrode (RHE) and showed at the top of the graph.

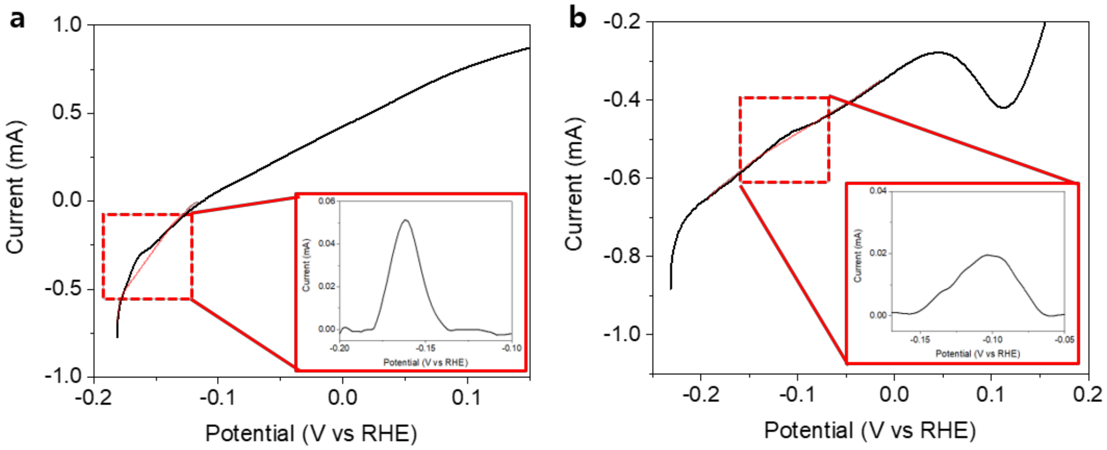

Fig. S4 Lead underpotential deposition curves on Cu catalysts on (a) CP and (b) GC. Each showed 3.42 cm^2 and 3.15 cm^2, respectively.

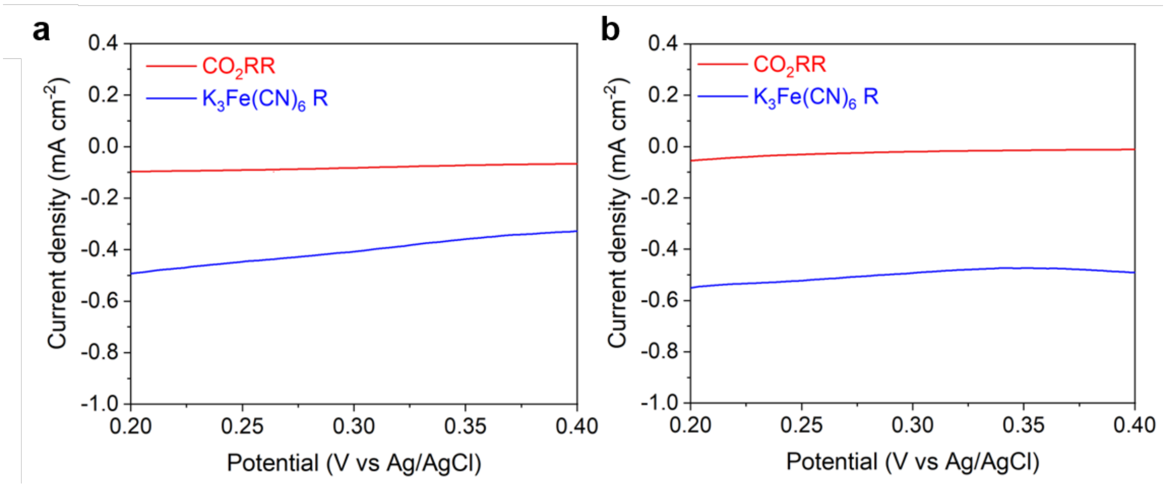

Fig. S5 LSVs of Cu catalysts deposited on (a) CP and (b) GC at potential range from 0.4 to 0.2 V obtained in CO_2 saturated 0.1 M $KHCO_3$ with (blue) and without (red) addition of 10 mM $K_3Fe(CN)_6$. The current densities of the $K_3Fe(CN)_6$ reduction for CP and GC were 0.41 mA cm^{-2} and 0.52 mA cm^{-2}, respectively.

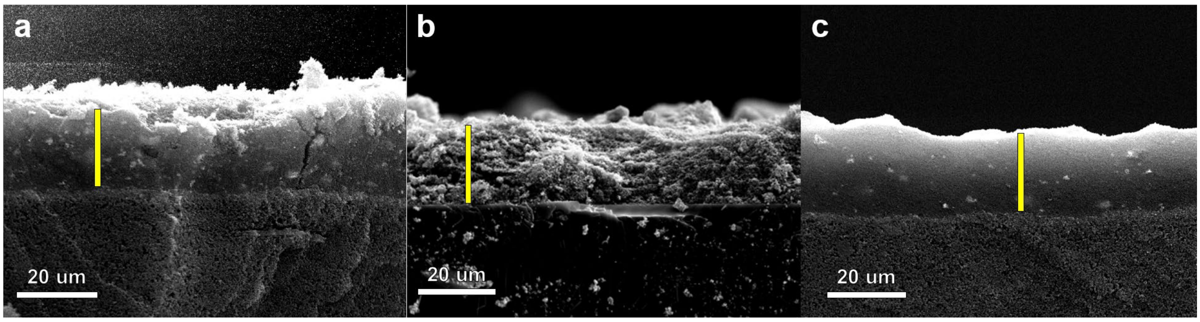

Fig. S6 Cross sectional SEM images of catalysts deposited on substrates. Cu (40 wt.% Cu_2O) catalyst on (a) CP and (b) GC, (c) Ag (16.7 wt.% Ag) catalyst on CP. 1 mg cm^{-2} of catalyst was sprayed. The thickness of the layers was (a) 20.77 µm, (b) 20.65 µm and (c) 21.92 µm.

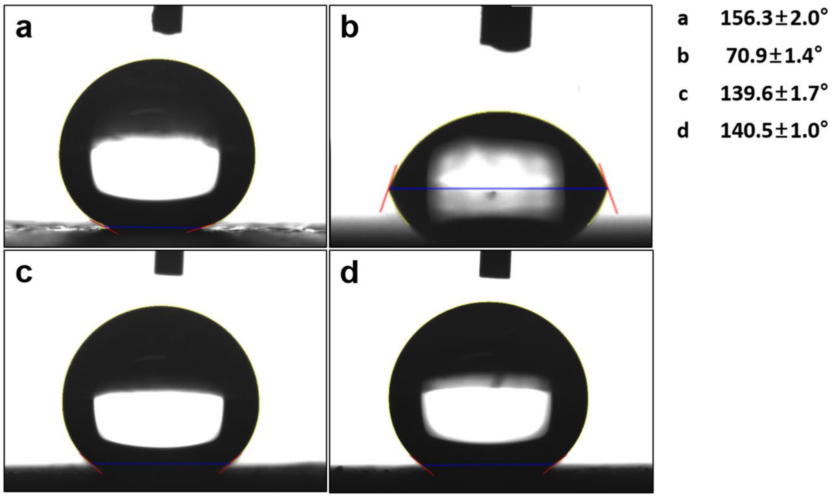

Fig. S7 The image of water contact angle. (a) bare CP, (b) bare GC, (c) Cu catalyst on CP and (d) Cu catalyst on GC. The angles were 156.3±2.0°, 70.9±1.4°, 139.6±1.7°, and 140.5±1.0°, respectively.

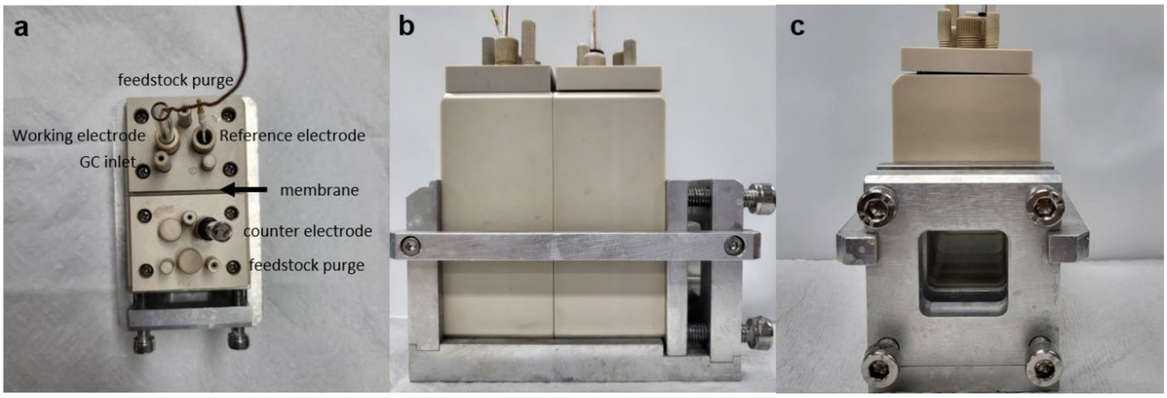

Fig. S8 Digital images of H-type cell made of polyetheretherketone. (a) top, and (b, c) side view. Catholyte and anolyte are separated by Selemion AMV-N ion exchange membrane. Working electrode and reference electrode are at the catholyte side and counter electrode is at the anolyte side. Each part is purged with feedstock gas (CO_2 or CO) by using 1/16” Teflon lines, which are directly inserted into the electrolytes at the location marked as ‘Gas inlet’ in Fig. 3b. The gas is discharged to ‘gas outlet’ at the top of the cell and analyzed by gas chromatography.

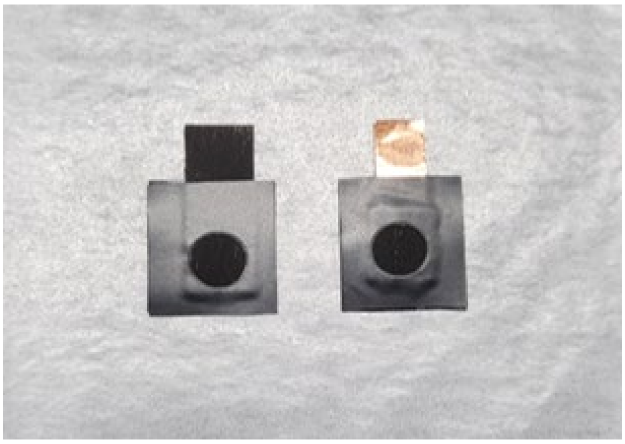

Fig. S9 Digital images of the carbon paper electrode (left) and the sealed carbon paper electrode (right). The porous layer was blocked by silicone tape and the copper tape was used for conductivity.

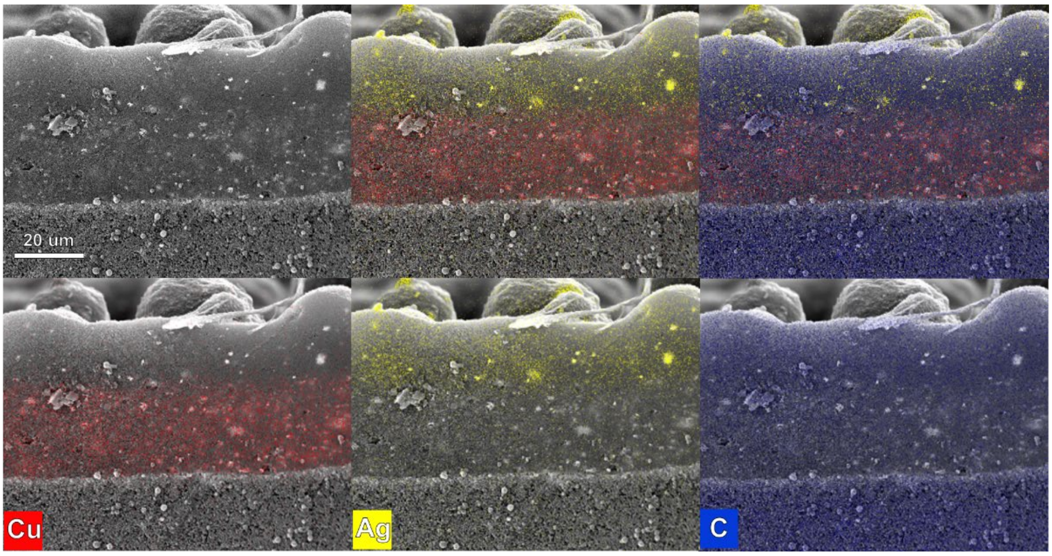

Fig. S10 Cross sectional SEM images of CP/Cu/Ag. Each 1 mg cm^{-2} of Cu catalyst and Ag catalyst was sprayed in order. The total thickness of the layers was 48.12 µm.

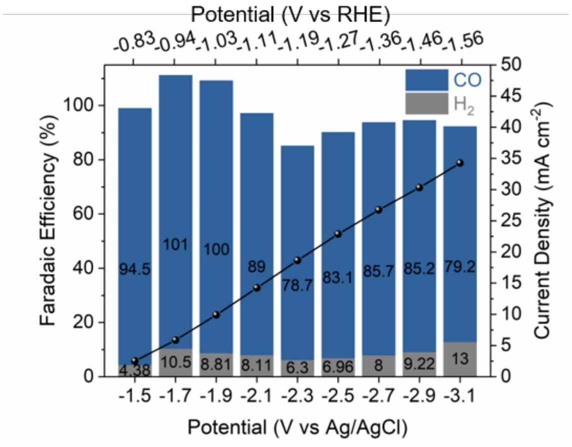

Fig. S11 CO_2RR performance of Ag catalyst in H-type cell: Faradaic Efficiencies of CO (blue) and H_2 (gray), current densities (black) at various potentials from -1.5 to -3.1 V vs. Ag/AgCl in CO_2-bubbled 0.1 M $KHCO_3$.

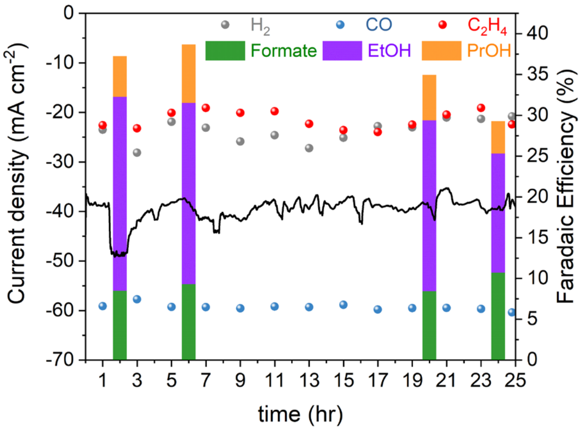

Fig. S12 CO_2RR performance of CP/Cu/Ag at -3.1 V vs. Ag/AgCl over time. The gas products, H_2 (gray), CO (blue), and C_2H_4 (red) were analyzed frequently, while liquid products, formate (green), ethanol (violet), and propanol (orange) were analyzed occasionally. The liquid products were analyzed 1 h after electrolyte exchange without stopping potentiostat.

Supplementary Tables

Table S1 The results of every experiment in this work, including the Faradaic efficiencies of every individual product including gases and liquids.

	Potential		Current density (mA cm^{-2})	Faradaic Efficiency (%)						
	V vs Ag/AgCl	V vs RHE		H_2	CO	C_2H_4	formate	PrOH	acetate	EtOH
carbon paper CO_2RR	-2.1	-1.0	18.6	18.6	28.9	20.3	4.9	3.1	1.1	15.4
glassy carbon CO_2RR	-2.1	-1.1	13	43.1	0.7	24.2	3.4	1.9	0.6	19.8
carbon paper CORR	-2.1	-1.1	13.7	37.3	-	37.4	-	6.4	2	14.8
glassy carbon CORR	-2.1	-1.2	9	93.2	-	2.9	-	-	-	-
sealed carbon paper CO_2RR	-2.1	-1.0	19	44.9	4.6	22.5	3.1	1.9	0.4	16.8
sealed carbon paper CORR	-2.1	-1.2	9	92.6	-	2.7	-	-	-	-
CP/Cu/Ag	-3.1	-1.4	36	26.3	8.5	29	6.3	4.1	1.9	27.1
CP/Ag/Cu	-3.1	-1.3	41.6	30.3	13.1	22.7	9.1	4.3	1.2	19.5
GC/Cu/Ag	-2.1	-1.2	11.4	50.2	5.6	15.5	8.8	3.4	-	12.4
GC/Ag/Cu	-2.1	-1.2	11.8	48.8	1.9	22.8	1.4	1.6	-	10.6

Table S2 The literature survey of the previous studies that conducted CO_2RR in H-type cells using copper catalysts and glassy carbons as substrates.

Catalyst	Substrate	Potential	Electrolyte	Counter electrode	Membrane	FE_{CO} (%)	FE_{C2+} (%)	$FE_{C2+/CO}$	Ref.
Cu_2O nanocubes	glassy carbon	-2.1 $V_{Ag/AgCl}$	0.1 M $KHCO_3$	Pt plate	Selemion AMV-N	0.7	46.5	66.4	This work
Cu_2O nanocubes	sealed carbon paper	-2.1 $V_{Ag/AgCl}$	0.1 M $KHCO_3$	Pt plate	Selemion AMV-N	4.6	41.6	9.0	
OT-CuNNs	glassy carbon	-1.4 $V_{Ag/AgCl}$	0.5 M $KHCO_3$	Pt plate	Nafion 117	4	55	13.8	8
Cu_2O/NRGO	glassy carbon	-1.4 V_{RHE}	0.1 M $KHCO_3$	Pt sheet	Nafion 117	4	19.7	4.9	9
ER-Cu_5-LDH	glassy carbon	-1.2 V_{RHE}	0.1 M $KHCO_3$	Pt mesh	AEM	8	44.8	5.6	10
Cu_2O NP/C	glassy carbon	-1.1 V_{RHE}	0.1 M $KHCO_3$	Pt foil	Selemion AMV-N	1.6	73.9	46.2	11
Cu@CuO NP/C	glassy carbon	-1.1 V_{RHE}	0.1 M $KHCO_3$	Pt foil	Selemion AMV-N	1.3	44.5	34.2	
Cu/VC 40wt%	glassy carbon	-1.2 $V_{Ag/AgCl}$	0.1 M $KHCO_3$	Pt foil	Selemion AMV-N	1	47	47	12
Cu/SWNT 20wt%	glassy carbon	-1.2 $V_{Ag/AgCl}$	0.1 M $KHCO_3$	Pt foil	Selemion AMV-N	1	43	43	
Cu/KB 50wt%	glassy carbon	-1.2 $V_{Ag/AgCl}$	0.1 M $KHCO_3$	Pt foil	Selemion AMV-N	1	33	33	
Cu nanocubes	glassy carbon	-1.1 V_{RHE}	0.1 M $KHCO_3$	Pt foil	Selemion AMV-N	2.1	47.7	22.7	13
PcCu-Cu-O	glassy carbon	-1.2 V_{RHE}	0.1 M $KHCO_3$	Pt foil	Nafion 117	4	50	12.5	14
Cu-ade	glassy carbon	-1.4 V_{RHE}	0.1 M $KHCO_3$	Pt net	Nafion 117	3.5	51.7	14.8	15
31 μgcm^2 CuO_x	glassy carbon	-0.84 V_{RHE}	0.1 M $KHCO_3$	Pt mesh	Nafion	3	28	9.3	16
c-Cu_2O	glassy carbon	-1.1 V_{RHE}	0.5 M $KHCO_3$	Pt	AEM	7.5	38	5.1	17
o-Cu_2O	glassy carbon	-1.1 V_{RHE}	0.5 M $KHCO_3$	Pt	AEM	6	45	7.5	
t-Cu_2O	glassy carbon	-1.1 V_{RHE}	0.5 M $KHCO_3$	Pt	AEM	4	59	14.8	
Cu-AC	glassy carbon	-1.09 V_{RHE}	0.1 M $KHCO_3$	PT plate	Nafion 117	5.9	12.4	2.1	18
Cu-EC	glassy carbon	-1.06 V_{RHE}	0.1 M $KHCO_3$	PT plate	Nafion 117	2.7	15.2	5.6	
Cu-VC	glassy carbon	-1.08 V_{RHE}	0.1 M $KHCO_3$	PT plate	Nafion 117	2.3	12.1	5.3	
branched Cu_2O	glassy carbon	-1.0 V_{RHE}	0.1 M $KHCO_3$	Pt	Nafion 117	5	53	10.6	19
cubic Cu_2O	glassy carbon	-1.0 V_{RHE}	0.1 M $KHCO_3$	Pt	Nafion 117	3	32	10.7	

Table S3 The literature survey of the previous studies that conducted CO_2RR in H-type cells using copper catalysts and porous carbon papers as substrates.

Catalyst	Substrate	Potential	Electrolyte	Counter electrode	Membrane	FE_{CO} (%)	FE_{C2+} (%)	$FE_{C2+/CO}$	Ref
Cu_2O nanocubes	carbon paper	-2.1 $V_{Ag/AgC}$	0.1M $KHCO_3$	Pt plate	Nafion 117	28.9	39.9	1.4	This work
CuO	carbon paper	-1.25 V_{RHE}	0.1M $NaHCO_3$	graphite sheet	Nafion 117	26	26.1	1.0	20
CuO/CX-72	carbon paper	-1.25 V_{RHE}	0.1M $NaHCO_3$	graphite sheet	Nafion 117	22	20.5	0.9	
CuO/NxC-700oC	carbon paper	-1.25 V_{RHE}	0.1M $NaHCO_3$	graphite sheet	Nafion 117	12	42.3	3.5	
CuNPs	carbon paper	-1.03 V_{RHE}	1M $KHCO_3$	nickel foam	Fumasep FAA- 3pk-130	18	52.5	2.9	21
CuO	carbon paper	-1.0 V_{RHE}	0.1M $KHCO_3$	Pt foil	Selemion AMV-N	7.5	67.7	9.0	22
Ni-TCPP@Cu-MOF	carbon paper	-1.27 V_{RHE}	0.5M $KHCO_3$	Pt	Nafion 115	14.5	33.4	2.3	23
Cu-Cu_xO/CNT/$BCKBH_4$	carbon cloth	-1.9 V_{RHE}	0.5M $KHCO_3$		Selemion AMV-N	24	36	1.5	24
Cu-Cu_xO/CNT/$BCNaBH_4$	carbon cloth	-1.5 V_{RHE}	0.5M $KHCO_3$		Selemion AMV-N	37	40	1.1	
pCu	carbon paper	-0.98 V_{RHE}	0.1M $KHCO_3$	glassy carbon	Selemion AMV-N	21.2	27.4	1.3	25
1UVO Cu	carbon paper	-0.98 V_{RHE}	0.1M $KHCO_3$	glassy carbon	Selemion AMV-N	15.4	39.8	2.6	
5UVO Cu	carbon paper	-0.98 V_{RHE}	0.1M $KHCO_3$	glassy carbon	Selemion AMV-N	12.5	47.7	3.8	
7UVO Cu	carbon paper	-0.98 V_{RHE}	0.1M $KHCO_3$	glassy carbon	Selemion AMV-N	16.4	44.2	2.7	

Supplementary References

1. Sigracet 39 BB carbon paper property sheet, *Powering up fuel cells: Our gas diffusion layer (White paper)*, Fuel Cell Store.
2. L. M. Pant, S. K. Mitra and M. Secanell, *J. Power Sources*, 2012, **206**, 153-160.
3. J. G. Wijmans and R. W. Baker, *J. Membr. Sci.*, 1995, **107**, 1-21.
4. S. Yamada and H. Sato, *Nature*, 1962, **193**, 261-262.
5. O. C. David, D. Gorri, A. Urtiaga and I. Ortiz, *J. Membr. Sci.*, 2011, **378**, 359-368.
6. F. Nasirpouri, *Ionics*, 2011, **17**, 331-337.
7. E. L. Clark, J. Resasco, A. Landers, J. Lin, L.-T. Chung, A. Walton, C. Hahn, T. F. Jaramillo and A. T. Bell, *ACS Catalysis*, 2018, **8**, 6560-6570.
8. K. S. Xiang, F. F. Zhu, Y. C. Liu, Y. F. Pan, X. Y. Wang, X. Yan and H. Liu, *Electrochem. Commun.*, 2019, **102**, 72-77.
9. H. Ning, Q. Mao, W. Wang, Z. Yang, X. Wang, Q. Zhao, Y. Song and M. Wu, *J. Alloys Compd.*, 2019, **785**, 7-12.
10. N. Altaf, S. Liang, R. Iqbal, M. Hayat, T. R. Reina and Q. Wang, *J. CO_2 Util.*, 2020, **40**.
11. H. Jung, S. Y. Lee, C. W. Lee, M. K. Cho, D. H. Won, C. Kim, H. S. Oh, B. K. Min and Y. J. Hwang, *J. Am. Chem. Soc.*, 2019, **141**, 4624-4633.
12. O. A. Baturina, Q. Lu, M. A. Padilla, L. Xin, W. Li, A. Serov, K. Artyushkova, P. Atanassov, F. Xu, A. Epshteyn, T. Brintlinger, M. Schuette and G. E. Collins, *ACS Catal.*, 2014, **4**, 3682-3695.
13. A. Loiudice, P. Lobaccaro, E. A. Kamali, T. Thao, B. H. Huang, J. W. Ager and R. Buonsanti, *Angew. Chem. Int. Ed.*, 2016, **55**, 5789-5792.
14. X. F. Qiu, H. L. Zhu, J. R. Huang, P. Q. Liao and X. M. Chen, *J. Am. Chem. Soc.*, 2021, **143**, 7242-7246.
15. F. Yang, A. Chen, P. L. Deng, Y. Zhou, Z. Shahid, H. Liu and B. Y. Xia, *Chem. Sci.*, 2019, **10**, 7975-7981.
16. X. Wang, A. S. Varela, A. Bergmann, S. Kuhl and P. Strasser, *ChemSusChem*, 2017, **10**, 4642-4649.
17. Y. Gao, Q. Wu, X. Liang, Z. Wang, Z. Zheng, P. Wang, Y. Liu, Y. Dai, M. H. Whangbo and B. Huang, *Adv. Sci.*, 2020, **7**, 1902820.
18. D. Choukroun, N. Daems, T. Kenis, T. Van Everbroeck, J. Hereijgers, T. Altantzis, S. Bals, P. Cool and T. Breugelmans, *J. Phys. Chem.*, 2020, **124**, 1369-1381.
19. J. Kim, W. Choi, J. W. Park, C. Kim, M. Kim and H. Song, *J. Am. Chem. Soc.*, 2019, **141**, 6986-6994.
20. H. J. Yang, H. Yang, Y. H. Hong, P. Y. Zhang, T. Wang, L. N. Chen, F. Y. Zhang, Q. H. Wu, N. Tian, Z. Y. Zhou and S. G. Sun, *ChemSusChem*, 2018, **11**, 881-887.
21. J. Wicks, M. L. Jue, V. A. Beck, J. S. Oakdale, N. A. Dudukovic, A. L. Clemens, S. Liang, M. E. Ellis, G. Lee, S. E. Baker, E. B. Duoss and E. H. Sargent, *Adv. Mater.*, 2021, **33**, e2003855.
22. S. Y. Lee, S. Y. Chae, H. Jung, C. W. Lee, D. L. T. Nguyen, H.-S. Oh, B. K. Min and Y. J. Hwang, *J. Mater. Chem.*, 2020, **8**, 6210-6218.
23. T. Yan, J. H. Guo, Z. Q. Liu and W. Y. Sun, *ACS Appl. Mater. Interfaces*, 2021, **13**, 25937-25945.
24. L. Gao, Y. Zhou, L. Li, L. Chen, L. Peng, J. Qiao and F. F. Hong, *Sep. Purif. Technol.*, 2022, **280**, 119832.
25. Y. Oh, J. Park, Y. Kim, M. Shim, T.-S. Kim, J. Y. Park and H. R. Byon, *J. Mater. Chem.*, 2021, **9**, 11210-11218.